Supplemental Information

Supplemental Figure and Table Legends

Figure S1. Measures of frequently used cognitive and pathology scoring for LOAD in ROS/MAP participants in this study, related to Figure 1. Shown are data relaying (A) MMSE, (B) global pathology, (C) Braak score, and (D) CERAD score. Shown in red are individuals with a clinical and neuropathological diagnosis of AD. Samples are ordered by global cognition at last visit. E) Table of metrics with statistical tests comparing individuals for whom iPSC lines were generated relative to the larger cohorts. Histograms showing the distribution of age at death (F), neuritic plaque score (G), and tau tangle score (H). Pie charts showing distribution across categories (I), sex (J), and APOE haplotype (K). Histograms showing distribution of global cognition at the last visit prior to death (L), the slope of global cognition over age (M) and MMSE score at last visit (N). LP=low pathology, no pathological AD diagnosis, HP=high pathology, pathological AD diagnosis, NCI=not cognitively impaired, AD= Alzheimer's dementia diagnosis.

Figure S2. Overview of quality control standards of ROSMAP iPSC lines required for inclusion in this study, related to Figure 1. A) Table of QC standards. B) Cell line expansion strategy for generating large numbers of synchronized d21 iN cultures while keeping passage numbers low.

Figure S3. Quality control metrics of iPSCs and neuronal differentiation, related to Figure 2. (A) Mean doubling time is graphed for each iPSC line and shows that doubling times are consistent with pluripotent stem cells and consistent across lines. Shown is mean +/-SD. Number of wells analyzed for each line is shown. (B) Heat map showing relative expression of cell fate markers in iNs across lines, determined mass spectrometry. There were no significant differences in cell fate marker gene expression between iNs derived from NCI and AD individuals (t-test, with Holm-Sidak multiple comparisons test; q-values all >0.75). (C-F) Example Incucyte analysis of cell density and neurite length over differentiation time. Following thaw at d4 of NGN2-induced differentiation, cells were counted and plated at equivalent densities (n=3 wells per line) and monitored for quality control purposes in an Incucyte automated live cell imaging incubator every 2 hours for 4 days. Cell body number and neurite length per cell body number were calculated, and those lines falling outside of 2 SD from the mean density were excluded from further analysis. Shown here is a representative example for such an analysis showing neurite length over time (C) and cell body cluster number over time (D). These analyses show no evidence for differences across categories in either cell body number or neurite length (E,F).

Figure S4. Differential RNA and protein expression between males and females in iNs and brain tissue, related to Figure 3.
(A) RNAseq data from iNs were examined to determine genes differentially expressed between males and females. Out of 16,597 genes quantified, 43 showed differential expression ($q<0.05$), volcano plot shown. Of these, 10 (shown in red) also are differentially expressed in the brain between males and females (ROS/MAP RNAseq data from PFC, differential expression determined following regression for RIN, PMI, age and diagnosis). Volcano plot of RNAseq analysis in brain shown in (B). (C-H) Examples of genes differentially expressed both in iNs and brain are shown: (C,F) XIST, (D,G) PUDP, and (E,H) USP9Y. (I) Proteomic data was acquired from iNs, and differential protein expression determined between males and females, two-stage linear step-up procedure of Benjamini, Krieger and Yekutieli. Volcano plot (I) shows proteins

showing a trend toward differential protein expression in iNs, in red are those proteins that are also differentially expressed in the postmortem brain. J) Proteomic data from human brain (ROS/MAP) was analyzed to examine male versus female differences (256 female, 115 male; 4,291 proteins analyzed). K-P) Examples of comparisons of protein expression between males and females in both iNs and brain: K,N) UBA1, L,O) SYAP1, and M,P) USP9X.

Figure S5. Differential protein expression and gene ontology analysis between NCI and AD iNs and brain tissue, related to Figure 4. (A) PCA plots of RNAseq and proteomics for iNs and brain datasets. All data was used to generate the PCA blots. AD individuals do not cluster together in iNs or brain datasets. B-K) Violin plots of a subset of proteins identified by analyses comparing LP-NCI and AD and HP- NCI vs AD showing data from iNs (B-F) and DLPFC (G-K). Significance determined by Kruskal- Wallis test with Dunn's multiple comparison's test. L) GO enrichment analyses of proteins differentially expressed between LP-NCI and AD in iNs ($p<0.05$) showed enrichment in terms related to protein localization and translation. This enrichment was driven in part by a reduction of a large number of ribosomal proteins of both the 40S and 60S subunits when comparing AD to LP-NCI iNs. In addition, proteins relevant to intracellular transport and localization were enriched in AD iNs. We then compared the proteomics GO enrichment observed in iNs to terms enriched in a proteomic data set from postmortem ROSMAP brains (388 individuals) comparing LP-NCI vs AD. The same GO terms also were significantly enriched in the postmortem brain dataset. (M-N) Differential strength of connections within the skyblue module across diagnostic categories. The skyblue module was the only module found to be downregulated in AD iNs relative to both LP-NCI and HP-NCI iNs. In order to examine associations between proteins within this module across categories, Pearson correlation analysis was performed between proteins within the skyblue module with data from NCI or AD iNs. Heat maps of the correlation coefficients show stronger correlations between proteins in AD iNs (M) compared to NCI iNs (N), which is reflected in a significant change in the distribution of Pearson r values for AD vs LP-NCI and AD vs HP- NCI (O). Kruskal-Wallis test with Dunn's multiple comparisons test: LP-NCI vs AD $p<0.0001$; HP- NCI vs AD $p<0.0001$; LP-NCI vs HP-NCI $p=0.66$. (P-Q) In order to examine associations between proteins within each module and the relationship across modules, Pearson correlation coefficients were calculated between each protein present in the modules shown for both iNs (P) and brain (Q). Heat maps of correlation coefficients across proteins show that for some modules, there are highly concordant patterns of association within modules between brain and iNs while others (such as those enriched in glia cell genes) show no such concordance.

Figure S6. Consistency of Aβ measurements across independent NGN2-inducible iPSC lines from the same individuals and plating densities, related to Figure 5.
(A-D) We determined whether the extent to which the generation of NGN2-inducible lines and the differentiation batch affects the relative levels of Aβ measured. To this end, NGN2-inducible lines were independently generated over six months and differentiated multiple times to neuronal fates with different lots of NGN2-virus and media components for four parental iPSC lines. Aβ38, 40 and 42 were measured in the media of the cells following two days of conditioning. Across these two sets of NGN2-inducible lines, we found that the rank order of Aβ42 levels and the ratio of Aβ42 to Aβ40 levels (Aβ42:40) was identical. However, the absolute value of Aβ peptides was variable. We previously showed that this phenomenon is likely due to lot-to-lot variability in the ELISA kits and synthetic Aβ peptide standards used to quantify Aβ [11]. Therefore, the data acquired on Aβ levels were normalized to eliminate ELISA batch effects in all subsequent analyses. (E-I) Linear relationship between density of iN plating and Aβ levels. A potential confounding factor when comparing across cell lines is the final density of plating. Despite efforts to plate the same number of viable cells across lines, subtle

differences can still arise. Therefore, we assessed whether relative Aβ levels (e.g., 42:40) were sensitive to differences in cell density, and whether extracellular Aβ levels in the media were proportional to the density of the neuronal cultures. To examine the effects of density on extracellular Aβ levels, two iPSC lines were plated at increasing densities, and Aβ levels were measured in the media following 48 hours of conditioning. A linear relationship was observed, suggesting that the level of each Aβ species (38, 40 and 42) was directly proportional to the plating density. We found that density affects the relative levels of different Aβ species, with increasing densities to 50K cells per well of a 96-well plate showing slightly lower 42:40 ratio. However, plating cells above this level (2-fold higher) did not further affect Aβ 42:40 (I). Therefore, we conducted all subsequent experiments using a plating density of 50K cells per well of a 96 well plate. (J-K) Relative levels of Aβ peptides measured in this study. Shown are Aβ data (J) and sAPPα and sAPPβ data (K) acquired via ELISA from d21 iNs across several ROSMAP iPSC lines for a single experiment to relay the relative levels of Aβ peptides measured. Extracellular Aβ peptides n=51, intraAβ peptides n=39, sAPP species n=39. The caveat of these data is that relative measurements between Aβ37, 38, 40 and 42 are potentially confounded by differential aggregation of the standards. However, comparisons between extra and intra Aβ have no such confound.

Figure S7. Association of intraAβ42:40 and proteins involved in regulation of RNA, proteasome activity, cytoskeleton, and vesicle-mediated transport, related to Figure 5. IntraAβ42:40 shows the strongest association with neuritic plaque score, (r=0.45, p=0.0021). (A) Bar graph of intraAβ 42:40 for each individual across differentiations (mean +/- SEM shown). (B) Scatter plot of mean of IntraAβ 42:40 for each individual across the three pathology/diagnostic categories. One-way ANOVA with Tukey!s multiple comparisons test comparing across categories. *p=0.02,**p=0.002. C) Spearman correlation coefficients were calculated between intraAβ42:40 and proteomic data from iNs (n=39 individuals, 1115 proteins quantified). Dotted red lines show significance threshold with multiple comparisons ($p=4.5x10^{-5}$) and threshold for suggestive hits that were used in GO analysis (Table S4). (D,E) Individual data points for each line showing correlation between intraAβ42:40 and each two of the significant hits: TMEM35A (G) and SF3B2 (H). (F,G) Correlations between levels of APP cleavage products in d21 iNs. APP cleavage products were measured for iNs generated from 50 iPSC lines over 3-12 differentiation rounds (average of 7) with 2-3 wells quantified per differentiation. Following batch correction, a composite estimate was generated for each metric by taking the mean value across differentiation rounds. Spearman correlation coefficients between APP cleavage products across genetic backgrounds (i.e. different lines) were calculated and are plotted to show Spearman rho value (color of circle) and p-value (size of circle) (F,G). F) Extracellular levels of Aβ38, 40 and 42 were highly positively correlated with one another, while each were strongly negatively correlated with Aβ37. G) Full correlation plot of all APP cleavage products with each other.

Figure S8. Detection of HMW tau using additional tau antibodies in iPSC-derived neurons, related to Figure 5. In order to further characterize the HMW bands of tau detected in iNs, WBs were performed to compare the banding pattern observed in iNs (d21) compared to dual SMAD EB-derived neurons (d100). In addition to AT8 and K9JA, p217 (Genetex) and AT270 (pT181, ThermoFisher Scientific) tau antibodies also were employed. Red arrowheads point to area of HMW tau (>191 kDa MWM).

Figure S9. No association between age at PBMC collection or any single LOAD GWAS SNP with Aβ42:37 or tau, related to Figure 6. (A-C) Spearman correlations were calculated between age of PBMC collection and measures from iNs including Aβ42:37 (A), Tau aggregate

score (B) and Aβ+Tau aggregate score (C). (D) Table of rare coding variants found in genes associated with AD.(E) Volcano plot showing a lack of association of LOAD-associated GWAS SNPs with Aβ42:37. (F,G) Scatter plots showing relationships between APOE haplotype and tau aggregate score (F) or Aβ42:37 (G) measured in iNs, (trends not significant). (H) AIP protein levels in iNs across APOE haplotypes. (I) The top associated LOAD GWAS SNP with tau aggregate score was one at the CD2AP locus. Shown is a scatter plot of the tau aggregate score across iNs relative to copy number of this LOAD risk SNP.

Figure S10. APOE genotype does not affect phopho-tau levels in NGN2-iNs, related to Figure 7.
An isogenic series of iPSC lines (Alstem) were differentiated to neuronal fate via NGN2-induction. At d21 neurons were lysed and Western blots performed to quantify pTau (AT8) and tau levels (K9JA, Dako). Three independent differentiations were analyzed, with n=3 wells analyzed per differentiation. Shown are example WBs, and quantification of data. One-way ANOVA was perfomed with Tukey's mutiple comparisons test, p-values listed.

Figure S11. Protein phosphatase 1 (PP1) levels and activity regulate ptau levels in neurons, related to Figure 7. (A-B) Lysates of iNs from eight individuals spanning the range of PPP1CA expression were collected in an independent round of differentiation and levels of PPP1CA analyzed by Western blot. Rank order levels of PPP1CA were identical between Western blot and proteomics (Spearman r=1.0; $p<0.0001$). (C-E) INs derived from five IPSC lines were treated with tautomycin (1μM) or vehicle (DMSO) for 24 hrs (d20-d21). WBs performed to measure levels of proteome-wide phospho-ser/thr (C) and media analyzed by ELISA to measure Aβ levels (D). Data show mean +/-SEM from 7 differentiations, 5 iPSC lines (BR21, BR89, BR04, BR40, BR60), n=18 wells per condition, each line normalized to vehicle. Student's t-test, *$p<0.05$. In addition, WB were run to quantify p-tau and total tau from five LP-NCI lines and five AD lines. Example WBs from LP-NCI iNs are shown in Figure 7 and from AD lines here (E) and all data quantified in Fig.7. (F,G) qPCR was performed to quantify levels of PPP1CA and PPP1R1A RNA following treatment with TauT, PF-06442609 or FeFb (normalized to GAPDH). Treatment with TauT (1μM) for 24 hours significantly elevated PPP1CA RNA levels (F) with no effect on PPP1R1A (G). One-way ANOVA with Tukey's multiple comparison's test, n=4-8, **** $p<0.0001$. (H) BR27 (AD) iNs were treated for the last two weeks of differentiation with PF0644206 or vehicle. For the last 48 hr, a subset of these treated wells also were treated with TauT (1μM). Following treatments, cells wer lysed and tau analyzed by WB. Shown are the mean +/-SEM, n=6, One-way ANOVA with Tukey's multiple comparison's test. *$p<0.05$, **$p<0.005$. (I) AD iNs were treated with 10 uM C2-ceramide for 48 hours and then lysed and tau analyzed by WB. Data shows mean +/-SEM, n=3-6 wells per condition, data normalized to vehicle within each line.

Figure S1.

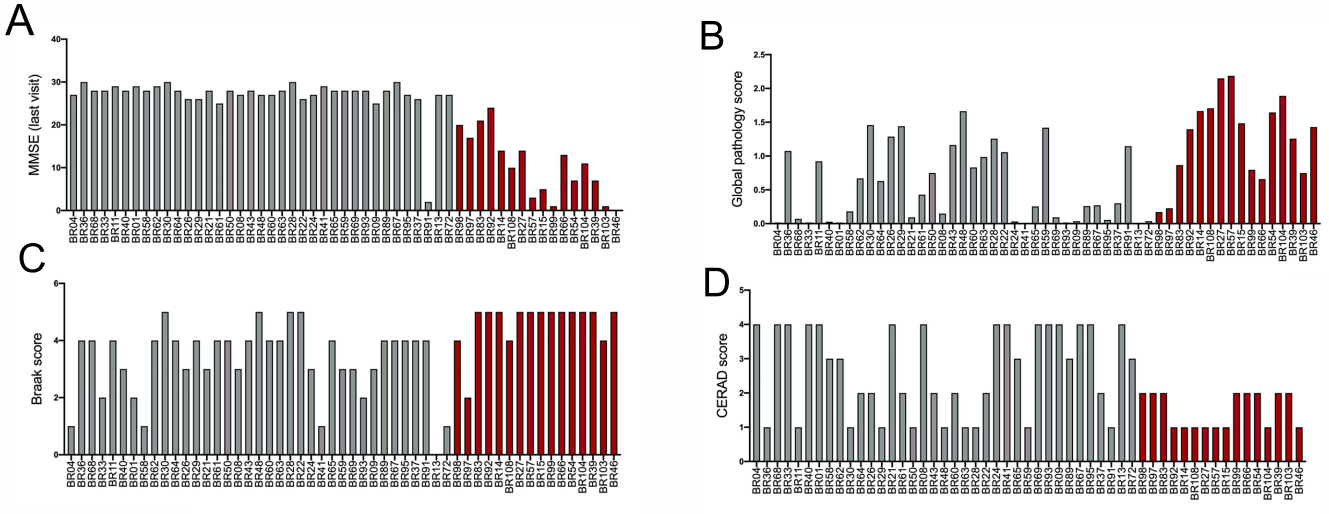

E

	All Deceased	This Study (iPSCs)	p-value	test
Category distribution (LPNCI, HPNCI, HPAD, LPAD)	30.1%,28.9%,33.7%,7.2%	37.8%,32.0%,30.2%,0%	0.16	Chi-square test
sex distribution (%F)	64.70%	69.80%	0.43	Chi-square test
age at death (mean +/- SD)	88.39 +/- 6.7	90.4 +/- 5.8	0.01	Welch's t-test
Neuritic plaque score (mean +/- SD)	0.56 +/- 0.59	0.89 +/- 1.1	0.15	Mann-Whitney test
Tau tangles score (mean +/- SD)	6.3 +/- 7.6	6.3 +/- 0.83	0.87	Mann-Whitney test
APOE genotype			0.75	Chi-square test
Global cognition-last visit			0.0015	Mann-Whitney test
Global cognition-slope			0.0003	Mann-Whitney test
MMSE - last visit			0.1	Mann-Whitney test

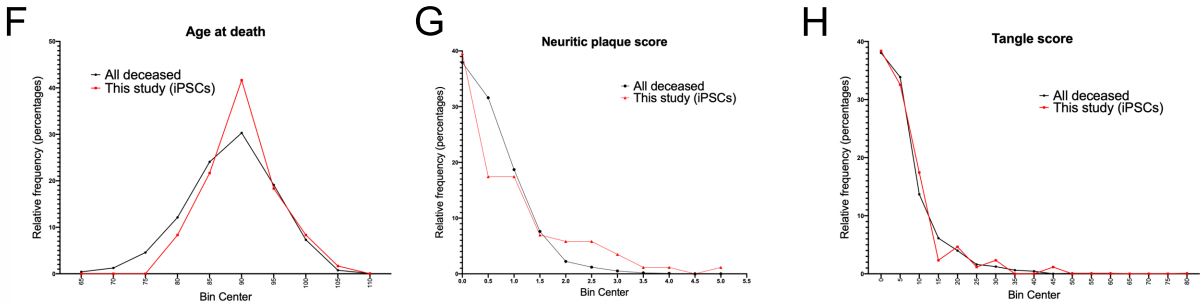

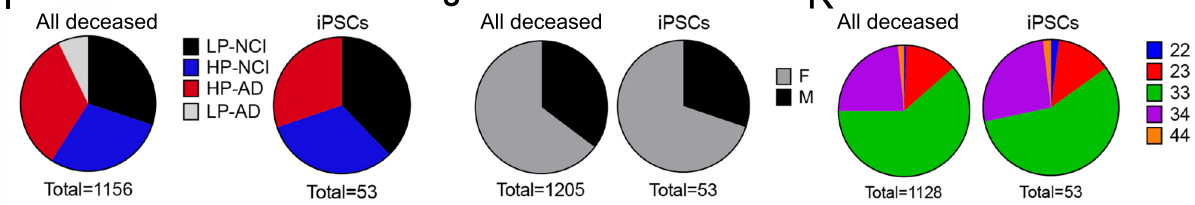

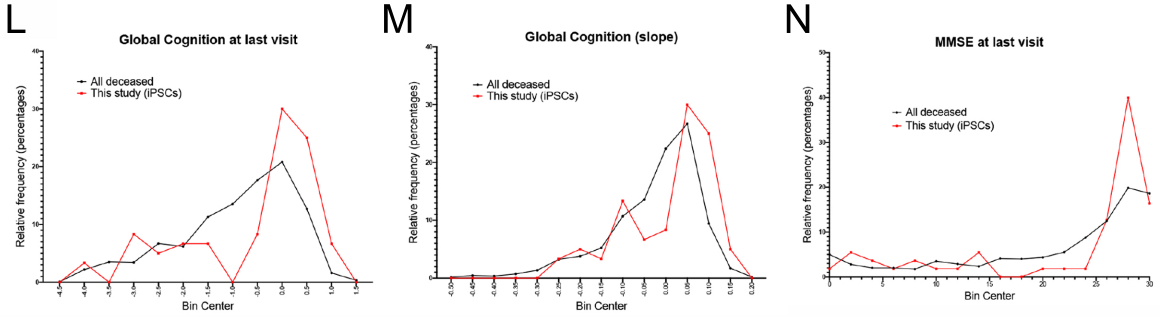

Figure S2.

A

Test Description	Test Method	Test Specification
Post-Thaw Viable Cell Recovery	Automated cryotube thaw to 6 well plate	>50% Confluency within 10 days
Sterility	SteriTEQ	Negative
Mycoplasma	Lonza MycoAlert Plus	Negative
Karyotype	Illumina CoreExome-24	Normal Karyotype (No Autosomal CNVs > 2.5MB)
Identity Match	Fluidigm SNPTrace Analysis	Match parent fibroblast line
Pluripotency Expression profile	Nanostring Pluripotency Scorecard Analysis	Express Markers of pluripotency with absence of early differentiation markers
Shutoff Sendai transgenes	Nanostring Gene Expression Analysis	Absence of Sendai Virus Expression
Differentiation Capacity	Nanostring 3 Germ Layer Scorecard Analysis	Absence of bias differentiation into any of three germ layers

B

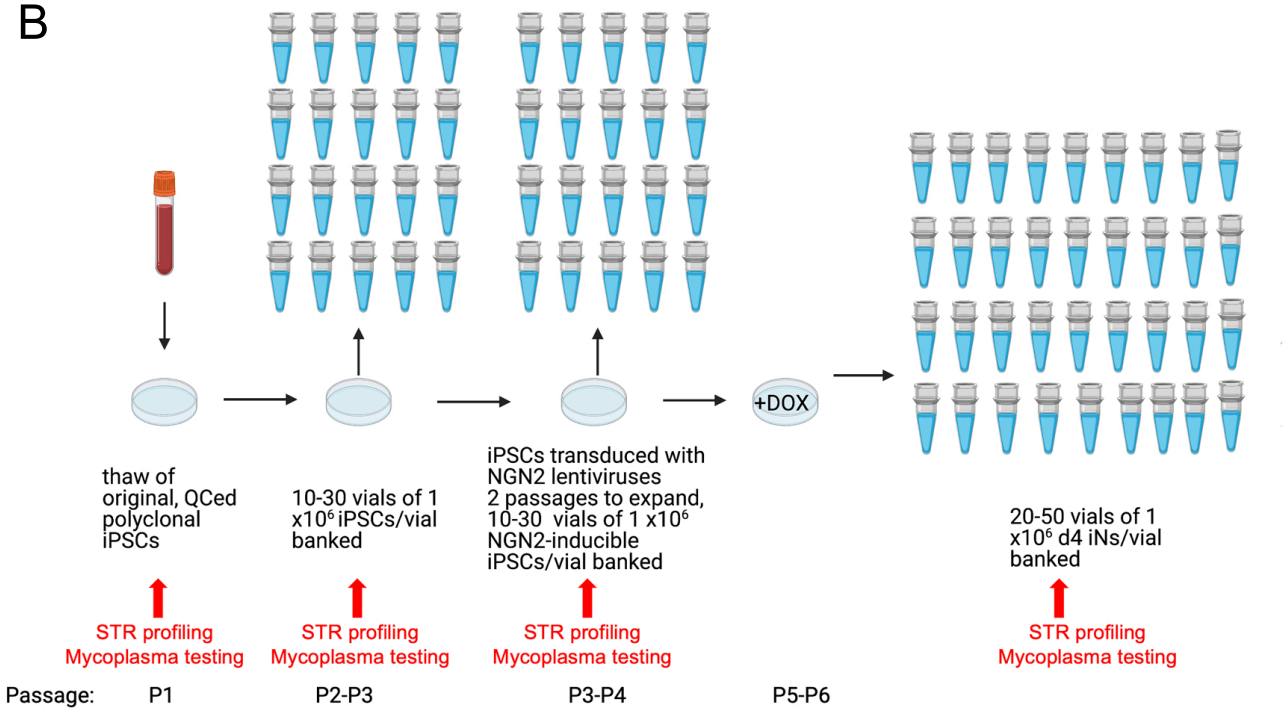

Figure S3.

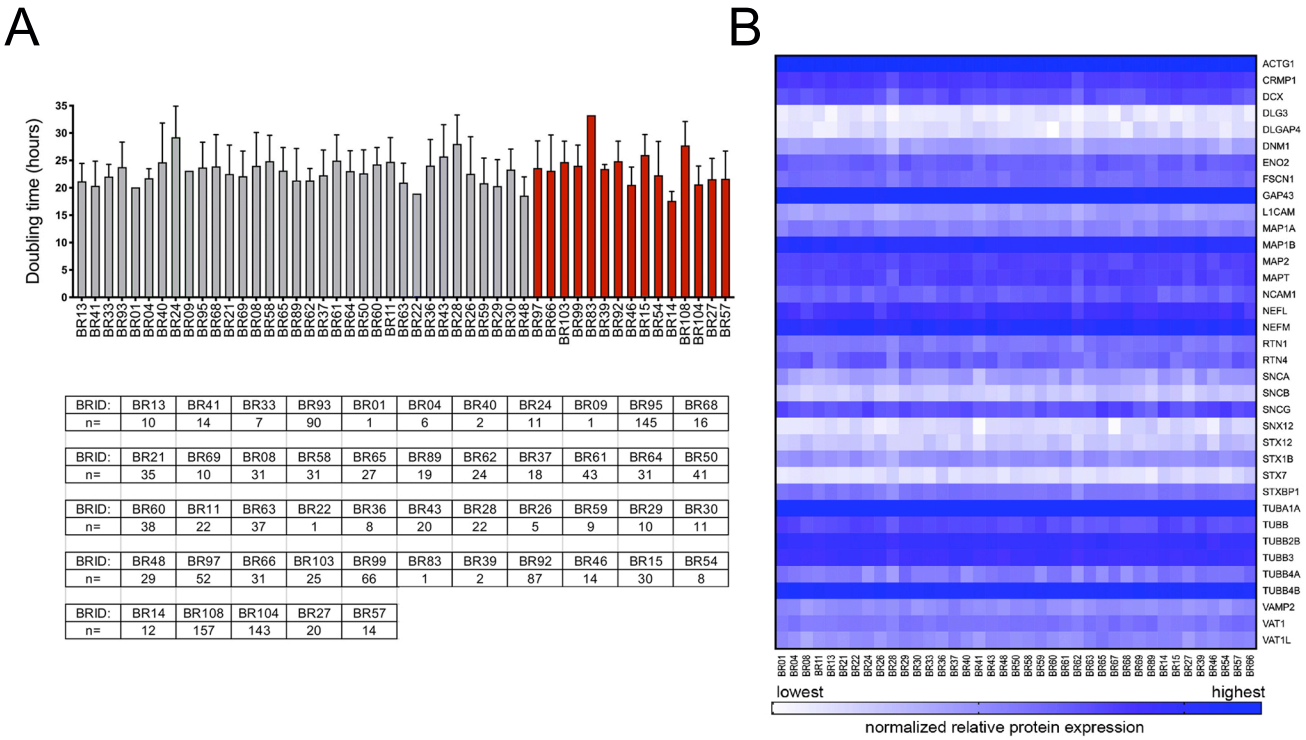

BRID:	BR13	BR41	BR33	BR93	BR01	BR04	BR40	BR24	BR09	BR95	BR68
n=	10	14	7	90	1	6	2	11	1	145	16

BRID:	BR21	BR69	BR08	BR58	BR65	BR89	BR62	BR37	BR61	BR64	BR50
n=	35	10	31	31	27	19	24	18	43	31	41

BRID:	BR60	BR11	BR63	BR22	BR36	BR43	BR28	BR26	BR59	BR29	BR30
n=	38	22	37	1	8	20	22	5	9	10	11

BRID:	BR48	BR97	BR66	BR103	BR99	BR83	BR39	BR92	BR46	BR15	BR54
n=	29	52	31	25	66	1	2	87	14	30	8

BRID:	BR14	BR108	BR104	BR27	BR57
n=	12	157	143	20	14

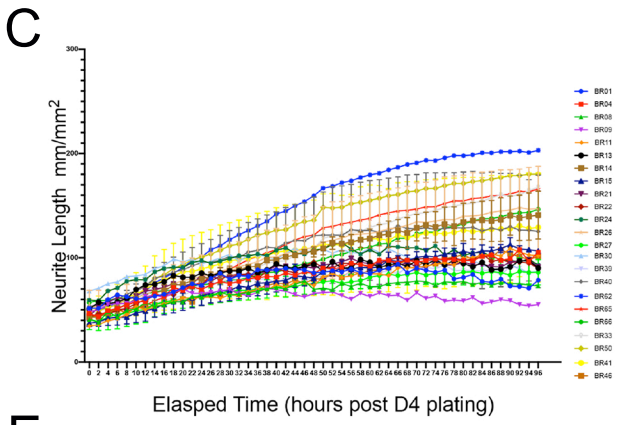

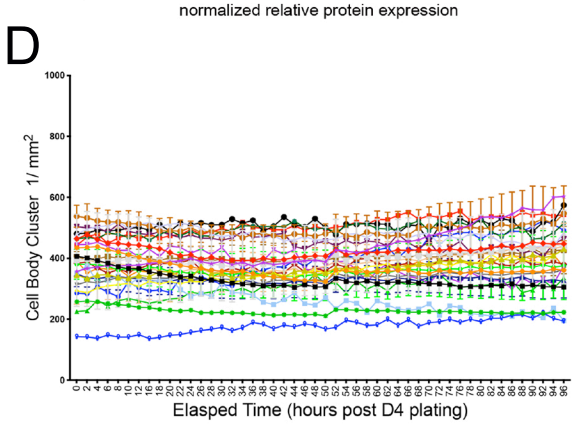

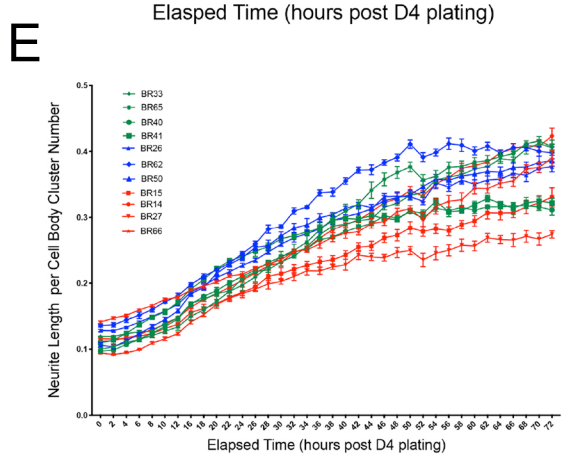

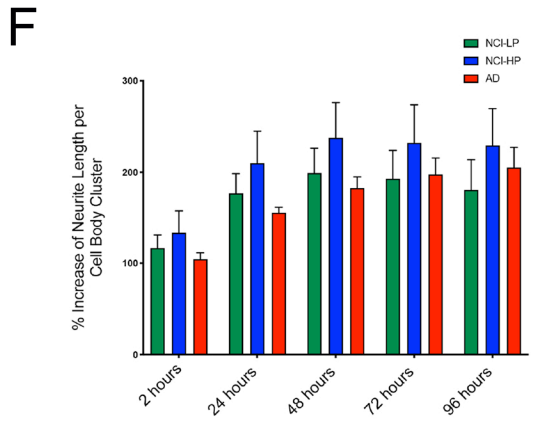

Figure S4.

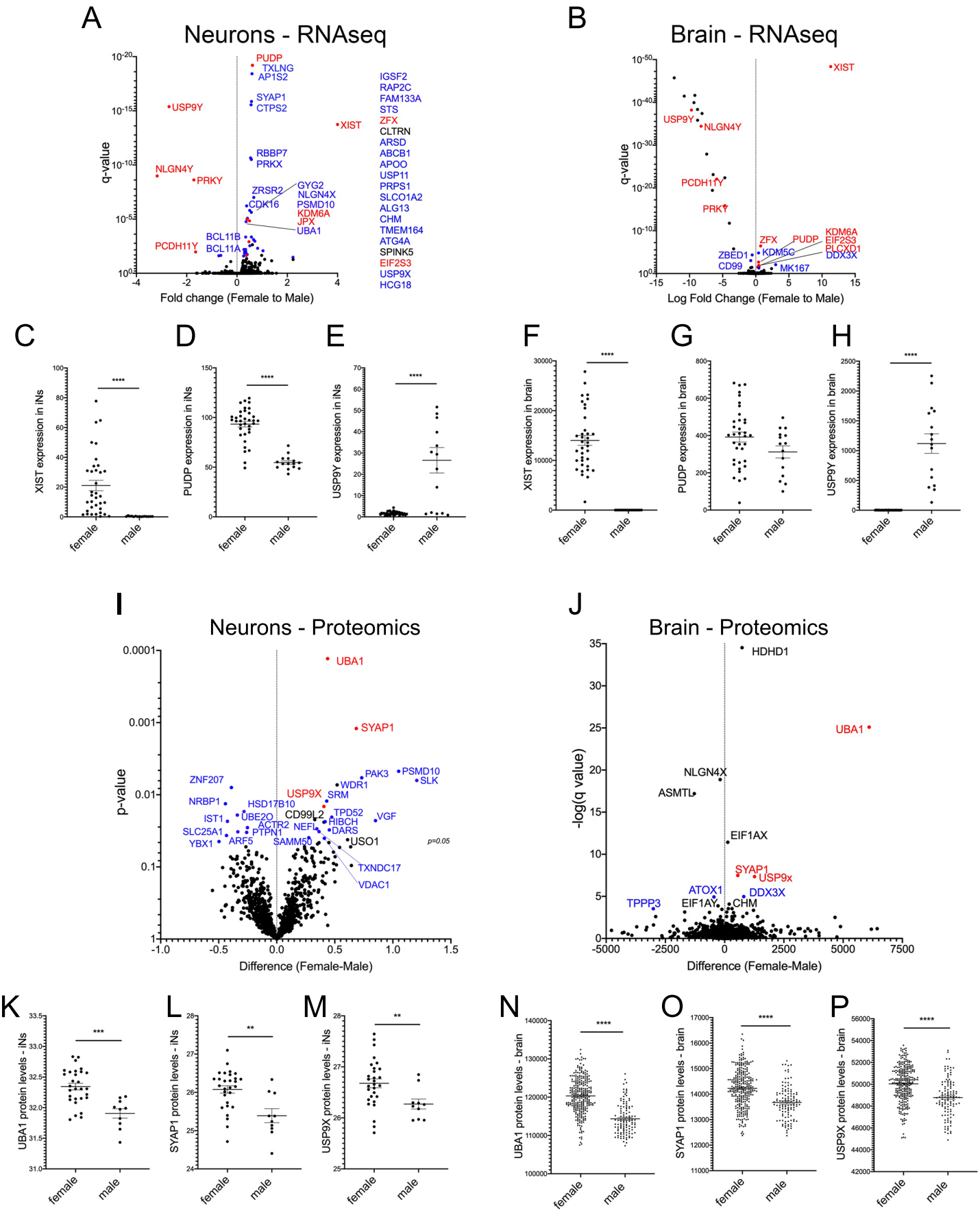
A
Neurons - RNAseq
q-value
Fold change (Female to Male)
PUDP
TXLNG
AP1S2
SYAP1
CTPS2
USP9Y
XIST
RBBP7
PRKX
NLGN4Y
PRKY
ZRSR2
GYG2
NLGN4X
CDK16
PSMD10
KDM6A
JPX
UBA1
BCL11B
PCDH11Y
BCL11A
IGSF2
RAP2C
FAM133A
STS
ZFX
CLTRN
ARSD
ABCB1
APOO
USP11
PRPS1
SLCO1A2
ALG13
CHM
TMEM164
ATG4A
SPINK5
EIF2S3
USP9X
HCG18
B
Brain - RNAseq
q-value
Log Fold Change (Female to Male)
XIST
USP9Y
NLGN4Y
PCDH11Y
PRKY
ZFX
PUDP
KDM6A
EIF2S3
PLCXD1
DDX3X
ZBED1
KDM5C
CD99
MK167
C
XIST expression in iNs
D
PUDP expression in iNs
E
USP9Y expression in iNs
F
XIST expression in brain
G
PUDP expression in brain
H
USP9Y expression in brain
****
female
male
I
Neurons - Proteomics
p-value
Difference (Female-Male)
UBA1
SYAP1
PAK3
PSMD10
SLK
ZNF207
WDR1
USP9X
SRM
NRBP1
HSD17B10
IST1
UBE2O
CD99L2
TPD52
VGF
ACTR2
NEFL
HIBCH
SLC25A1
PTPN1
DARS
YBX1
ARF5
SAMM50
USO1
p=0.05
TXNDC17
VDAC1
J
Brain - Proteomics
-log(q value)
Difference (Female-Male)
HDHD1
UBA1
NLGN4X
ASMTL
EIF1AX
SYAP1
USP9x
ATOX1
DDX3X
TPPP3
EIF1AY
CHM
K
UBA1 protein levels - iNs
L
SYAP1 protein levels - iNs
M
USP9X protein levels - iNs
N
UBA1 protein levels - brain
O
SYAP1 protein levels - brain
P
USP9X protein levels - brain
***
**
****
female
male

Figure S5.

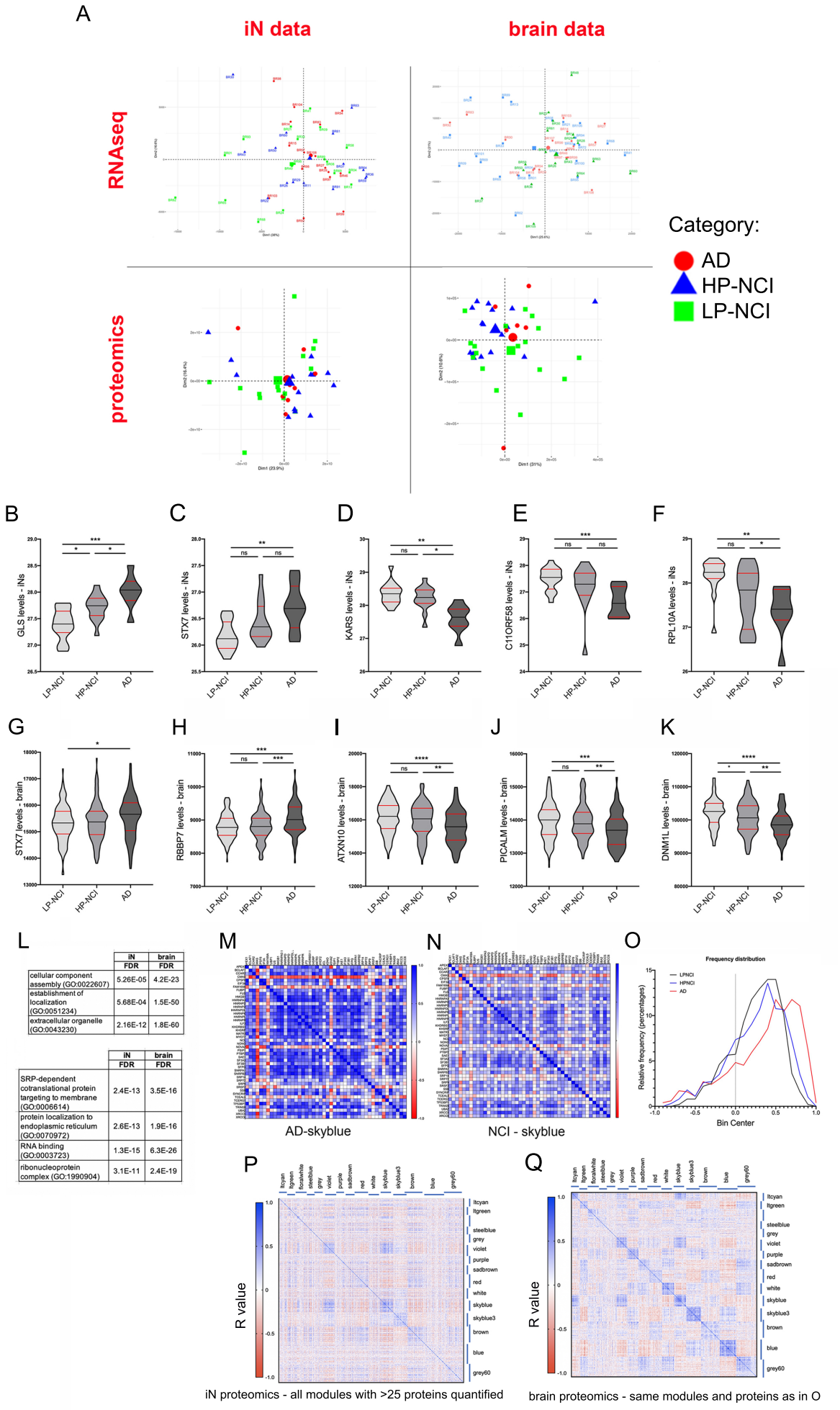

	iN FDR	brain FDR
cellular component assembly (GO:0022607)	5.26E-05	4.2E-23
establishment of localization (GO:0051234)	5.68E-04	1.5E-50
extracellular organelle (GO:0043230)	2.16E-12	1.8E-60

	iN FDR	brain FDR
SRP-dependent cotranslational protein targeting to membrane (GO:0006614)	2.4E-13	3.5E-16
protein localization to endoplasmic reticulum (GO:0070972)	2.6E-13	1.9E-16
RNA binding (GO:0003723)	1.3E-15	6.3E-26
ribonucleoprotein complex (GO:1990904)	3.1E-11	2.4E-19

Figure S6.

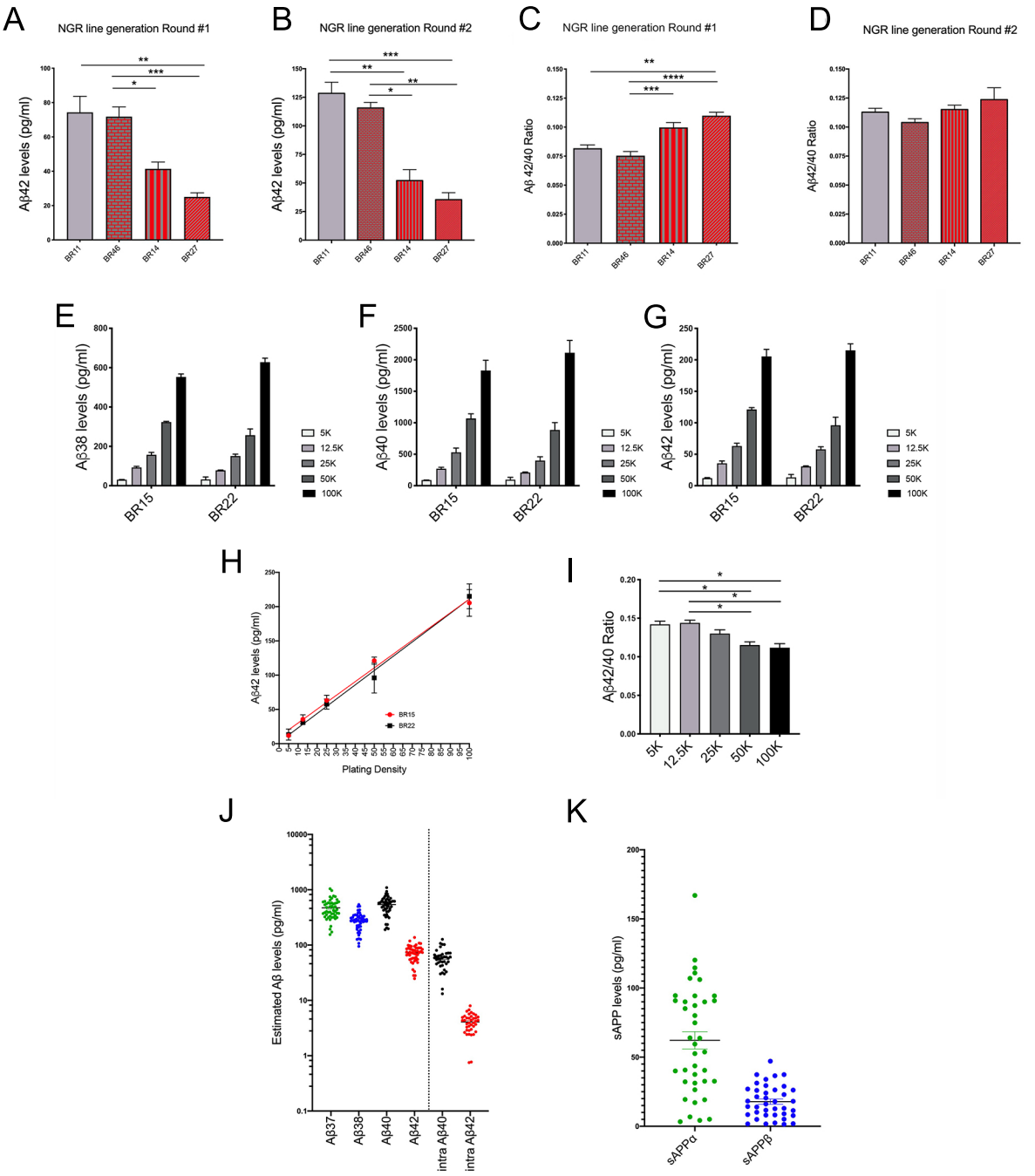
A
NGR line generation Round #1
Aβ42 levels (pg/ml)
BR11
BR46
BR14
BR27
B
NGR line generation Round #2
Aβ42 levels (pg/ml)
C
NGR line generation Round #1
Aβ 42/40 Ratio
D
NGR line generation Round #2
Aβ42/40 Ratio
E
Aβ38 levels (pg/ml)
BR15
BR22
5K
12.5K
25K
50K
100K
F
Aβ40 levels (pg/ml)
G
Aβ42 levels (pg/ml)
H
Aβ42 levels (pg/ml)
Plating Density
I
Aβ42/40 Ratio
J
Estimated Aβ levels (pg/ml)
Aβ37
Aβ38
Aβ40
Aβ42
intra Aβ40
intra Aβ42
K
sAPP levels (pg/ml)
sAPPα
sAPPβ

Figure S7.

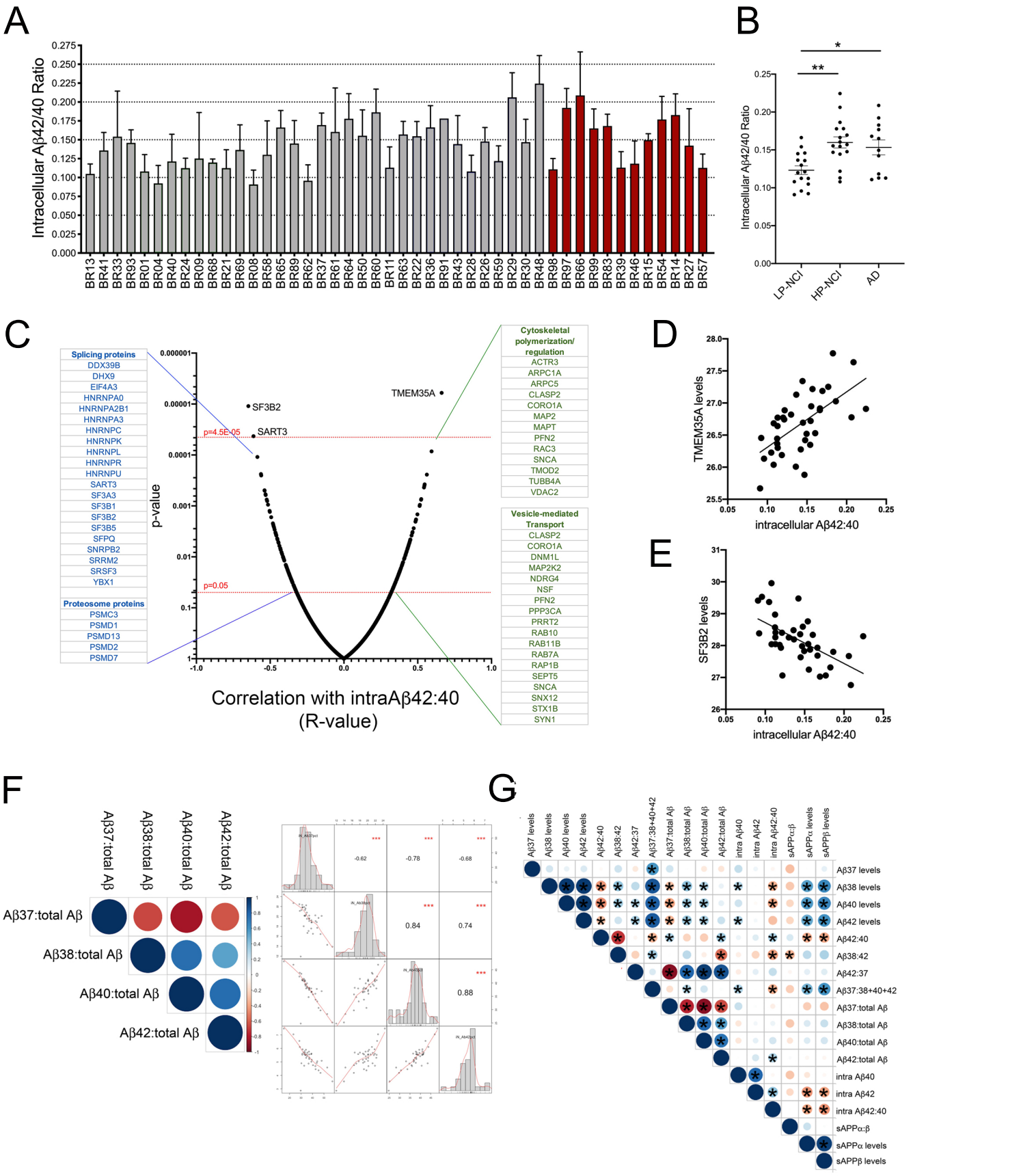
A
Intracellular Aβ42/40 Ratio
BR13 BR41 BR33 BR93 BR01 BR04 BR40 BR24 BR09 BR68 BR21 BR69 BR08 BR58 BR65 BR89 BR62 BR37 BR61 BR64 BR50 BR60 BR11 BR63 BR22 BR36 BR91 BR43 BR28 BR26 BR59 BR29 BR30 BR48 BR98 BR97 BR66 BR99 BR83 BR39 BR46 BR15 BR54 BR14 BR27 BR57
B
Intracellular Aβ42/40 Ratio
LP-NCI
HP-NCI
AD
C
Splicing proteins
DDX39B
DHX9
EIF4A3
HNRNPA0
HNRNPA2B1
HNRNPA3
HNRNPC
HNRNPK
HNRNPL
HNRNPR
HNRNPU
SART3
SF3A3
SF3B1
SF3B2
SF3B5
SFPQ
SNRPB2
SRRM2
SRSF3
YBX1
Proteosome proteins
PSMC3
PSMD1
PSMD13
PSMD2
PSMD7
SF3B2
SART3
TMEM35A
p=4.5E-05
p=0.05
p-value
Correlation with intraAβ42:40
(R-value)
Cytoskeletal polymerization/ regulation
ACTR3
ARPC1A
ARPC5
CLASP2
CORO1A
MAP2
MAPT
PFN2
RAC3
SNCA
TMOD2
TUBB4A
VDAC2
Vesicle-mediated Transport
CLASP2
CORO1A
DNM1L
MAP2K2
NDRG4
NSF
PFN2
PPP3CA
PRRT2
RAB10
RAB11B
RAB7A
RAP1B
SEPT5
SNCA
SNX12
STX1B
SYN1
D
TMEM35A levels
intracellular Aβ42:40
E
SF3B2 levels
intracellular Aβ42:40
F
Aβ37:total Aβ
Aβ38:total Aβ
Aβ40:total Aβ
Aβ42:total Aβ
-0.62
-0.78
-0.68
0.84
0.74
0.88
G
Aβ37 levels
Aβ38 levels
Aβ40 levels
Aβ42 levels
Aβ42:40
Aβ38:42
Aβ42:37
Aβ37:38+40+42
Aβ37:total Aβ
Aβ38:total Aβ
Aβ40:total Aβ
Aβ42:total Aβ
intra Aβ40
intra Aβ42
intra Aβ42:40
sAPPα:β
sAPPα levels
sAPPβ levels

Figure S8.

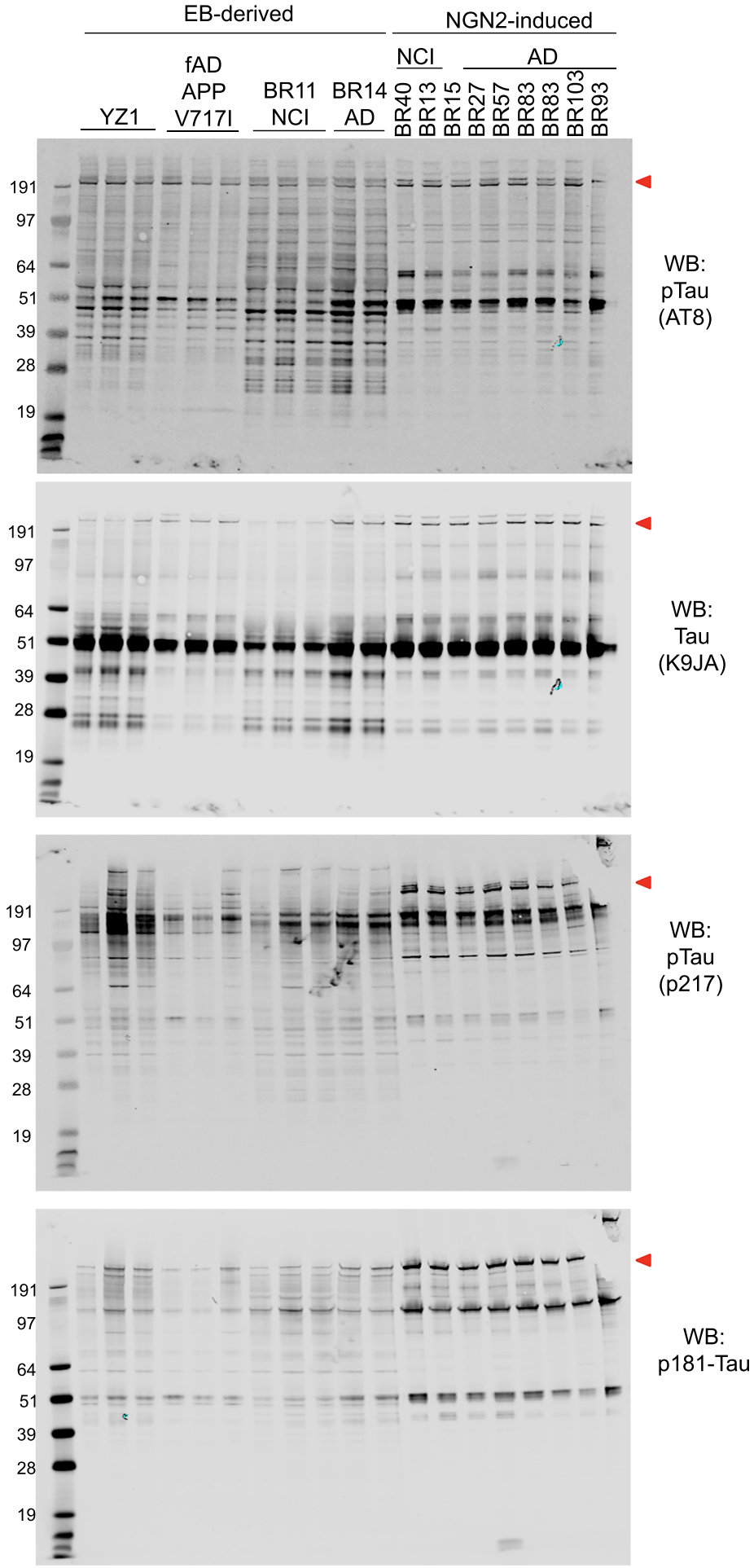
EB-derived
NGN2-induced
NCI
AD
YZ1
fAD APP V717I
BR11 NCI
BR14 AD
BR40
BR13
BR15
BR27
BR57
BR83
BR83
BR103
BR93
191
97
64
51
39
28
19
WB: pTau (AT8)
WB: Tau (K9JA)
WB: pTau (p217)
WB: p181-Tau

Figure S9.

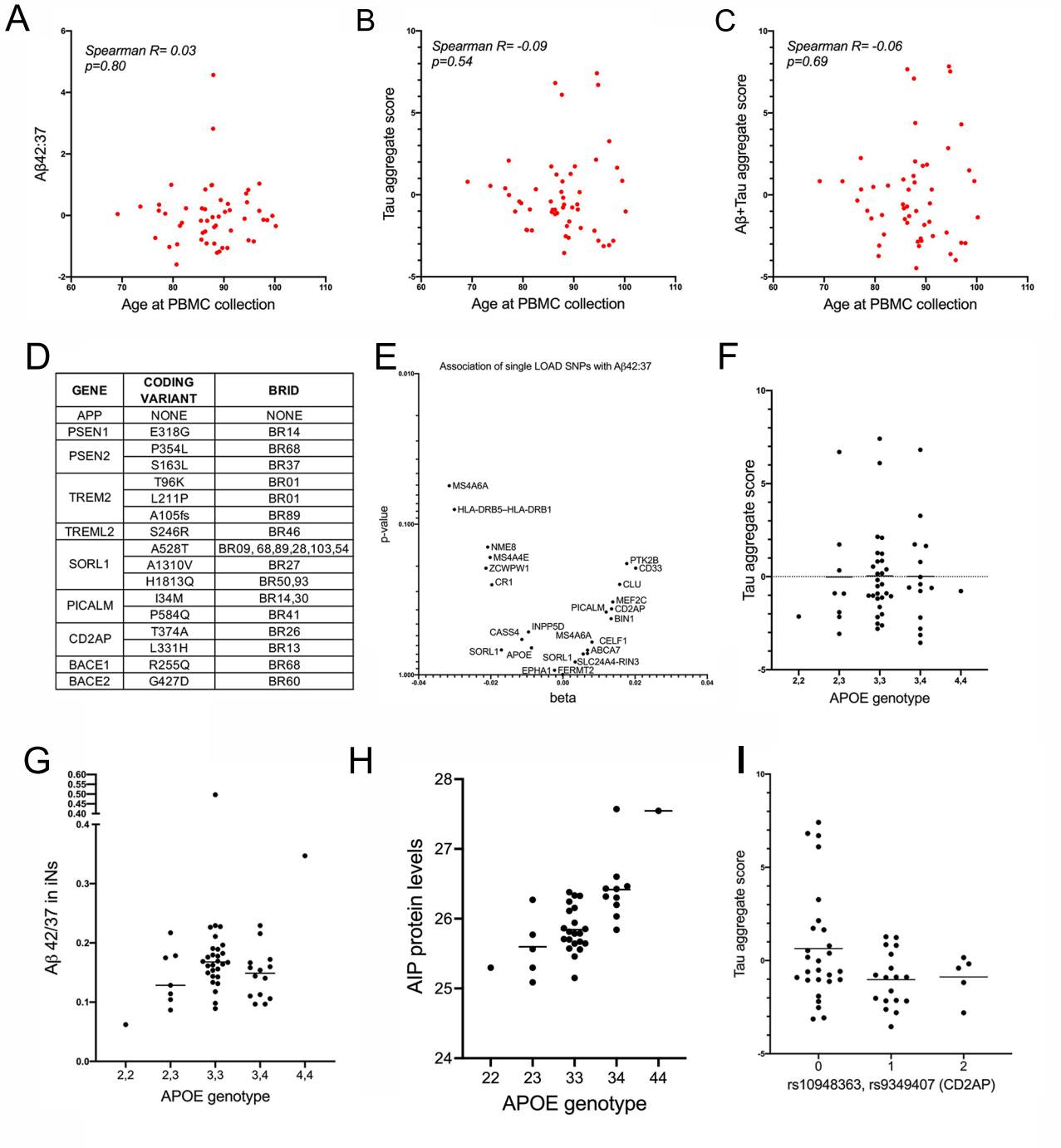

GENE	CODING VARIANT	BRID
APP	NONE	NONE
PSEN1	E318G	BR14
PSEN2	P354L	BR68
	S163L	BR37
TREM2	T96K	BR01
	L211P	BR01
	A105fs	BR89
TREML2	S246R	BR46
SORL1	A528T	BR09, 68,89,28,103,54
	A1310V	BR27
	H1813Q	BR50,93
PICALM	I34M	BR14,30
	P584Q	BR41
CD2AP	T374A	BR26
	L331H	BR13
BACE1	R255Q	BR68
BACE2	G427D	BR60

Figure S10.

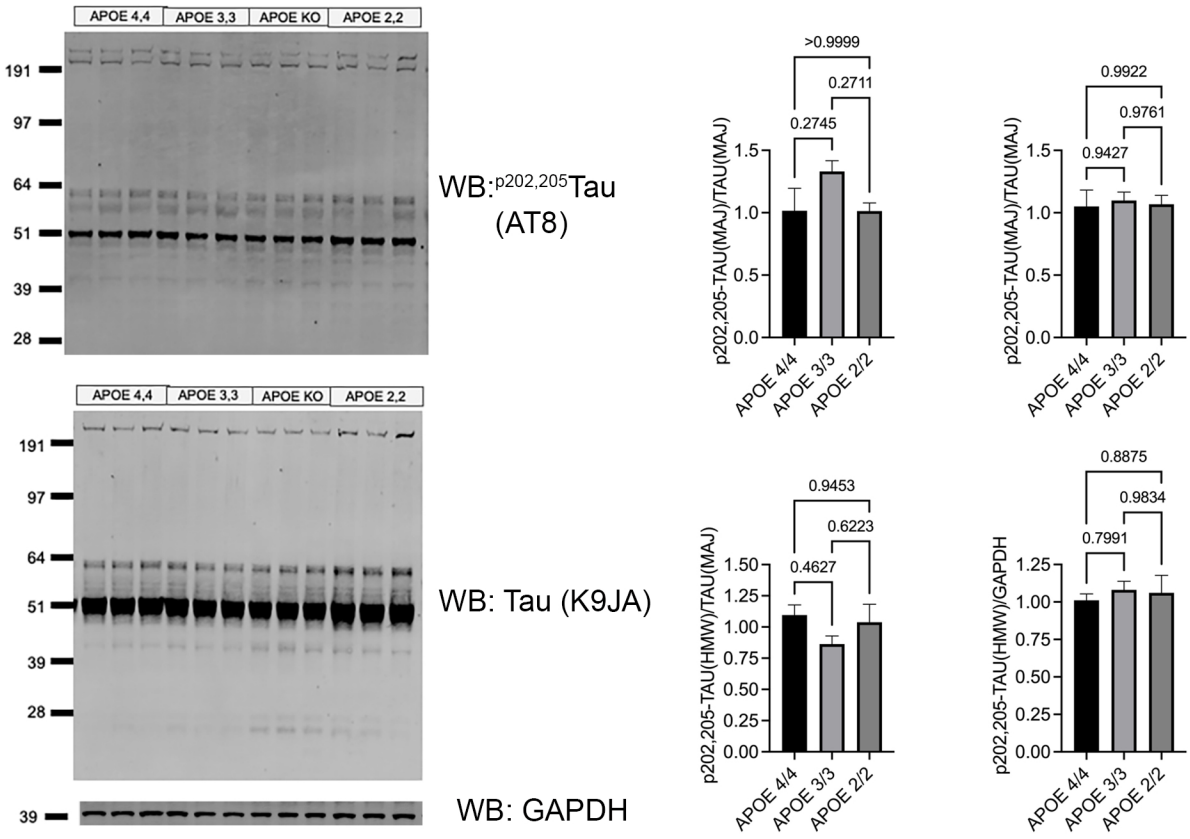
APOE 4,4
APOE 3,3
APOE KO
APOE 2,2
191
97
64
51
39
28
WB:p202,205Tau
(AT8)
WB: Tau (K9JA)
WB: GAPDH
>0.9999
0.2711
0.2745
p202,205-TAU(MAJ)/TAU(MAJ)
0.9922
0.9761
0.9427
0.9453
0.6223
0.4627
p202,205-TAU(HMW)/TAU(MAJ)
0.8875
0.9834
0.7991
p202,205-TAU(HMW)/GAPDH
APOE 4/4
APOE 3/3
APOE 2/2

Figure S11.

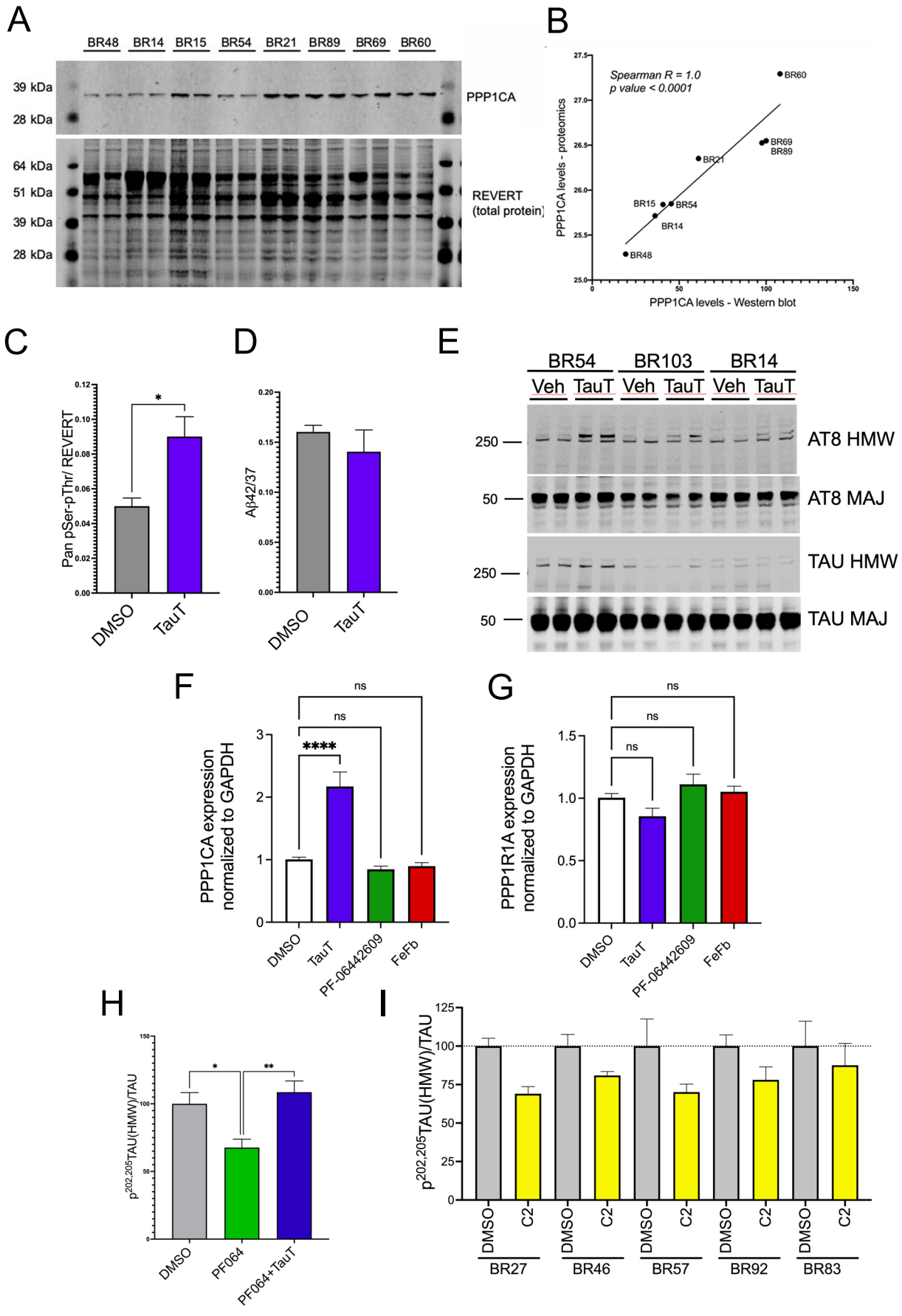
A
BR48 BR14 BR15 BR54 BR21 BR89 BR69 BR60
39 kDa
28 kDa
PPP1CA
64 kDa
51 kDa
39 kDa
28 kDa
REVERT
(total protein)
B
Spearman R = 1.0
p value < 0.0001
PPP1CA levels - proteomics
PPP1CA levels - Western blot
BR60
BR69
BR89
BR21
BR15
BR54
BR14
BR48
C
Pan pSer-pThr/ REVERT
DMSO
TauT
D
Aβ42/37
DMSO
TauT
E
BR54 BR103 BR14
Veh TauT Veh TauT Veh TauT
250
50
AT8 HMW
AT8 MAJ
250
50
TAU HMW
TAU MAJ
F
PPP1CA expression
normalized to GAPDH
ns
ns
****
DMSO
TauT
PF-06442609
FeFb
G
PPP1R1A expression
normalized to GAPDH
ns
ns
ns
DMSO
TauT
PF-06442609
FeFb
H
p202,205TAU(HMW)/TAU
*
**
DMSO
PF064
PF064+TauT
I
p202,205TAU(HMW)/TAU
DMSO
C2
BR27
BR46
BR57
BR92
BR83